Impact of RCM Spatial Resolution on the Reproduction of Local, Subdaily Precipitation

JONAS OLSSON AND PETER BERG

Research and Development (Hydrology), Swedish Meteorological and Hydrological Institute, Norrköping, Sweden

AKIRA KAWAMURA

Department of Civil and Environmental Engineering, Tokyo Metropolitan University, Tokyo, Japan

(Manuscript received 5 January 2014, in final form 4 November 2014)

ABSTRACT

Many hydrological hazards are closely connected to local precipitation (extremes), especially in small and urban catchments. The use of regional climate model (RCM) data for small-scale hydrological climate change impact assessment has long been nearly unfeasible because of the low spatial resolution. The RCM resolution is, however, rapidly increasing, approaching the size of small catchments and thus potentially increasing the applicability of RCM data for this purpose. The objective of this study is to explore to what degree subhourly temporal precipitation statistics in an RCM converge to observed point statistics when gradually increasing the resolution from 50 to 6 km. This study uses precipitation simulated by RCA3 at seven locations in southern Sweden during 1995–2008. A positive impact of higher resolution was most clearly manifested in 10-yr intensity–duration–frequency (IDF) curves. At 50 km the intensities are underestimated by 50%–90%, but at 6 km they are nearly unbiased, when averaged over all locations and durations. Thus, at 6 km, RCA3 apparently generates low-frequency subdaily extremes that resemble the values found in point observations. Also, the reproduction of short-term variability and less extreme maxima were overall improved with increasing resolution. For monthly totals, a slightly increased overestimation with increasing resolution was found. The bias in terms of wet fraction and wet spell characteristics was overall not strongly dependent on resolution. These metrics are, however, influenced by the cutoff threshold used to separate between wet and dry time steps as well as the wet spell definition.

1. Introduction

Hydrological simulation and prediction in small catchments depend strongly on input representing local precipitation at short (subhourly) time steps. This is particularly the case in urban environments, where the combination of small catchments (often below 1 km^2) and a large fraction of impervious surface makes the runoff process extremely fast. Usually, the precipitation input comes from a single gauge with a temporal resolution down to single seconds (e.g., a tipping bucket). At these resolutions, the temporal structure of precipitation is characterized by an extreme variability and a well-defined intermittency, accurately describing the alternating sequences of wet and dry spells (e.g., Restrepo-Posada and Eagleson 1982). The extremes are often characterized by constructing intensity–duration–frequency (IDF) curves, which are widely used in urban hydrological engineering and design (e.g., Maidment 1993). Climate change is generally expected to alter precipitation statistics, notably toward more intense extremes (e.g., Trenberth et al. 2007), and estimation of future statistics on the local scale is thus a key component for designing water management systems in a resilient and climate-proof way.

Small-scale hydrological climate change impact assessment is generally performed using results from regional climate models (RCMs). Although commonly available, RCM results typically have a daily resolution; the attainable RCM output time step may be close to the requirements for small-scale hydrology (e.g., 30 min; Olsson

Corresponding author address: Jonas Olsson, Research and Development (Hydrology), Swedish Meteorological and Hydrological Institute, Folkborgsvägen 17, 60176 Norrköping, Sweden.
E-mail: jonas.olsson@smhi.se

DOI: 10.1175/JHM-D-14-0007.1

et al. 2009). The typical spatial resolution (25–50 km) is, however, fundamentally different from the point scale, and the temporal structure of spatially averaged precipitation differs substantially from that of point-scale precipitation. To tackle this discrepancy, various methods to downscale the RCM results to local scale have been developed and applied. Approaches made include the Delta change concept, empirical transfer functions, weather type analyses, and conditional stochastic modeling [see Willems et al. (2012) for an overview].

The spatial resolution of RCMs is, however, constantly increasing, up to 5 km and even higher in recent experiments (e.g., Kendon et al. 2012; Chan et al. 2013). Higher resolution improves not only the land surface representation, such as steep topographical gradients, but also the possibility to simulate important small-scale precipitation processes. With increasing resolution, the dynamics of the RCM start to resolve deep convection. Most convective phenomena are generally considered to be sufficiently resolved at less than about 5-km horizontal grid spacing. This allows switching off parameterizations of deep convection, which is a large source of error in model simulations (e.g., Prein et al. 2013).

In several recent studies, the impact of an increased RCM resolution (and sometimes also changed setup) on precipitation characteristics has been evaluated, and in the following some examples are given. In terms of monthly or seasonal totals, van Roosmalen et al. (2010) investigated the impact of using 50-, 25-, and 12.5-km resolutions in a 30-yr run of HIRHAM, version 4, for Denmark. Generally, monthly totals increased with increasing resolution, which in most cases improved the agreement with observations, especially in summer. Tripathi and Dominguez (2013) used 10- and 50-km setups of the WRF Model and evaluated 32-yr simulations for the southwestern United States. Generally, precipitation amounts increased with increasing resolution, thereby increasing the wet bias, particularly in summer. Chan et al. (2013) found an improvement in especially orographic precipitation over Britain at 12 km compared to 50-km versions of the RCM Hadley Centre Global Environment Model, version 3–Regional Atmosphere (HadGEM3-RA). They also showed that the Met Office Unified Model at 1.5-km resolution (UKV model) was not clearly improving precipitation regarding average intensities, compared with the 12- and 50-km versions.

In terms of heavy precipitation and the diurnal cycle, two studies of 10-yr runs for southern England with a 12-km RCM (HadGEM3-RA) and a nested 1.5-km forecast model (UKV model) run in climate mode showed that very heavy precipitation (>99th percentile) was underestimated in the 12-km run but overestimated in the 1.5-km run (Kendon et al. 2012; Chan et al. 2013). Tripathi and Dominguez (2013) found that large (>90th percentile) 3- and 24-h summer events were better captured in the 10-km run than in the 50-km run. Berg et al. (2013b) investigated precipitation intensity distributions from two GCMs and several regional downscalings thereof with the models CLM, WRF, and Regional Model (REMO) over Germany at 50- and 7-km resolutions. They found the GCMs to perform rather well when compared to observations remapped to the same spatial resolution; however, at higher resolutions, the RCMs bring added value, and the 7-km simulations had extremes similar to observations. Walther et al. (2013) obtained an improved reproduction of the observed afternoon precipitation peak in Sweden when increasing the resolution of RCA3 from 50 to 6 km.

A key feature of temporal precipitation generally not considered in RCM evaluation is the clustering of wet time steps into events, separated by dry periods. It must be emphasized that the prospect of event separation and analysis is highly dependent upon the temporal resolution of the data. It is sometimes performed using daily data, by distinguishing between 1-day, 2-day, etc., events (e.g., Heinrich and Gobiet 2012). This is certainly doable, but with a daily time step the connections to the physical mechanisms of precipitation generation become weak. A wet day may represent precipitation anywhere between a few minutes (a short shower, or possibly several) and 24 h (a slowly propagating front); a 2-day event may in reality have been caused by a few minutes of precipitation around midnight. With a (sub)hourly time step, the time series' events represent their ''true'' characteristics and thus directly reflect the physical mechanisms. Analyzing event-based characteristics of subdaily RCM time series is therefore a potential way of diagnosing the model's ability to simulate the physical mechanisms (e.g., Haerter et al. 2010; Berg et al. 2013a), but to our knowledge, this approach has been used only to a very limited extent. Kendon et al. (2012) found a distinct improvement of both the duration of heavy precipitation events and the amount of dry spells in the 1.5-km run as compared with the 12-km run.

The objective of this paper is to add to current knowledge with respect to the impact of RCM spatial resolution on the reproduction of temporal precipitation statistics. This is achieved by using precipitation data from RCM runs at resolutions of 50, 25, 12.5, and 6.25 km and comparing with point observations from seven locations in southern Sweden. The key underlying question is to what degree the higher-resolution RCM runs are able to approach subdaily variability and extremes as estimated from point observations. Compared with previous studies we use (i) a higher, subhourly (30 min) temporal

resolution and (ii) a more complete suite of evaluation metrics that, besides conventional descriptive statistics, includes extreme statistics (IDF curves) and event-based measures (number, depth, and duration of wet spells). The results obtained are interpreted in terms of RCM limitations and future research needs.

2. Material and initial assessment

The main reference data comprise 30-min precipitation time series (accumulations) from seven locations in southern Sweden (Fig. 1; approximately 55°–60°N and 11°–19°E): Arvika (Arv), Göteborg (Göt), Gladhammar (Gla), Lidköping (Lid), Malmö (Mal), Stockholm (Sto), and Växjö (Väx). The area may be characterized as temperate rainy, without dry seasons but with warm summers (Johannessen 1970). The large-scale airflow is mainly southwesterly year-round, which brings warm, moist Atlantic air to the area. Over the area, air masses converge at the polar front, situated at 50°N as an annual average but shifting northward in summer and southward in winter. Cyclonic activity along the front is most intense in winter, because of greater temperature contrasts. Thus, large-scale synoptic convergence and frontal systems are the dominant mechanisms from autumn to spring, whereas in summer (mainly July and August) precipitation is also generated by mesoscale convection (e.g., Dai 2001).

The 30-min data come from a network of automatic stations managed by the Swedish Meteorological and Hydrological Institute, initiated in 1995. The selection was made with the dual aim of (i) covering as much as possible of southern Sweden and (ii) using gauges with a minimum of missing data. The gauges are of a weighing type (Geonor) with a resolution of 0.1 mm. Missing data amounted to 3.8%, and to obtain complete time series for the event-based analysis, missing periods were filled in by data from the same period in the nearest year that the gauge was functional, making sure no extreme values were copied in the procedure. The 30-min data were obtained by aggregating the original 15-min data two by two after careful quality control.

A second source of precipitation reference data is from the Precipitation and Temperature for the Hydrologiska Byråns Vattenbalansavdelning (HBV) model (PTHBV) database, comprising daily gridded ($4 \times 4\,\text{km}^2$) historical fields of precipitation and temperature over Sweden. The precipitation grid is created by optimal interpolation from all available stations, corrected for observation losses. In the interpolation scheme, topography as well as frequencies of wind direction and wind speed are taken into account (Johansson 2000; Johansson and Chen 2003).

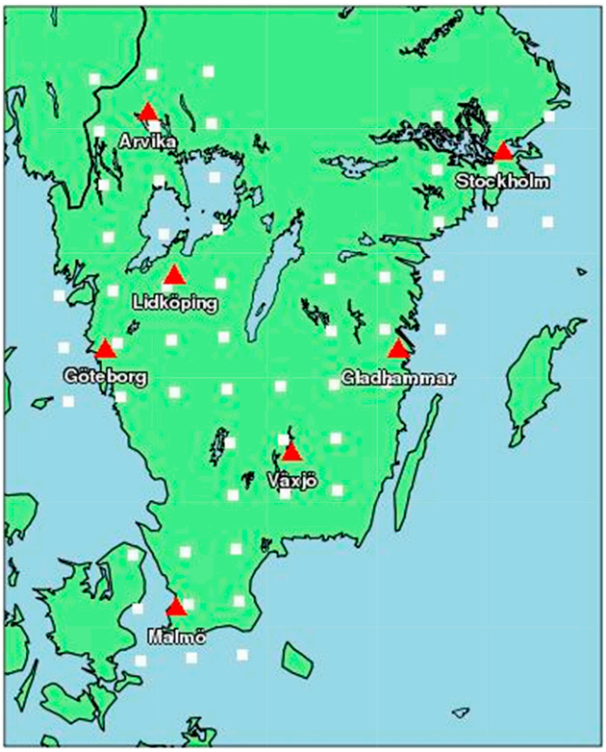

FIG. 1. Map of the investigation area in southern Sweden. Station locations are marked with a red triangle, and the surrounding clusters of nine white squares indicate the approximate $150 \times 150\,\text{km}^2$ area used for the RCM data.

Climate data from RCA3 (Kjellström et al. 2005; Samuelsson et al. 2011) have been used. In an experiment, the model was set up at four different spatial resolutions: 50×50, 25×25, 12.5×12.5, and $6.25 \times 6.25\,\text{km}^2$ (in the following, we refer to the different resolutions as 50, 25, 12, and 6 km). The simulations were performed over a period of several years, and some model development took place in between. Thus, the model code is not identical for all experiments, but the differences can be considered minor. RCA3 uses the Kain–Fritsch parameterization for convective processes (Kain and Fritsch 1993). This scheme has the advantage that it only parameterizes up- and downdrafts and not mesoscale motions, which are resolution dependent as they are resolved to a larger extent with increasing resolution (Jones et al. 2004). The domain was of all Europe (on the so-called ENSEMBLES grid) for all resolutions and the simulation period 1987–2008. The boundary fields in this simulation are based on the 40-yr European Centre for Medium-Range Weather Forecasts (ECMWF) Re-Analysis (ERA-40) until mid-2002 and operational ECMWF analyses during the rest of the simulation period. These simulations thus represent RCA3 performance under optimal forcing, as the boundary is to a large degree based on observed meteorological fields.

From the RCA3 simulations, 30-min precipitation time series from gridcell matrices centered over each location (Fig. 1) were extracted. The area covered is 150 × 150 km^2 (22 500 km^2), which corresponds to a 3 × 3 matrix (9 cells) at 50-km resolution, as shown in Fig. 1. To avoid spurious features and reduce statistical scatter, it is important to include more than single grid cells in the analysis. To ensure spatial consistency, data from the same 150 × 150 km^2 areas are used at the higher resolutions, corresponding to a 6 × 6 matrix (36 cells) at 25 km, 12 × 12 matrix (144 cells) at 12 km, and 24 × 24 matrix (576 cells) at 6 km. The gauge resolution 0.1 mm is also used as the cutoff threshold for the RCM data (i.e., all values <0.1 mm are set to zero), neglecting any impact of the gridcell area. The overlapping period used in the analysis below is 1995–2008.

Assessment of spatial realism

The subdaily temporal analyses below (section 3) are based on the hypothesis that at some high enough spatial resolution, precipitation statistics become effectively indistinguishable from point statistics. Our objective is to examine how this convergence is manifested in these RCM data. Therefore, we neglect any influence of RCM gridcell area but treat all RCM data as representing the point scale, performing exactly the same calculations as for the point observations without any adjustment. To justify this comparison of ''apples versus oranges,'' and to complement the point-scale analyses below, an initial assessment of the spatial realism in RCA3 was performed. In this assessment, PTHBV and RCA3 data during the entire period (1995–2009) in the 150 × 150 km^2 box surrounding station Växjö (Fig. 1) were compared. This is the only box that does not contain a substantial fraction of water (sea or lake), where PTHBV is not defined. PTHBV precipitation data were aggregated to approximate resolutions 12, 25, and 50 km, producing matrices very similar to the RCA3 ones at these resolutions. As the 6-km resolution cannot be attained by direct aggregation of PTHBV grid cells, to avoid interpolation effects, we do not consider this resolution in this assessment.

Two types of analyses were performed: spatial correlation function and spatial coefficient of variation. In the former, the correlation coefficient (CC) was first calculated between daily time series from all possible pairs of grid cells and then plotted as a function of separation distance. At the 12-km resolution, the data sources exhibit a very similar behavior with slightly convex functions decreasing from a CC of almost 1 at the minimum separation distance 12 km to CC ≈ 0.5 at the maximum distance of almost 200 km (Fig. 2a). The only difference is a slightly higher correlation for short distances in the PTHBV data. For both data sources, the correlation functions at resolutions of 25 and 50 km (not shown) are very similar to the ones at 12 km.

In the analysis of the coefficient of variation (CV; ratio of standard deviation to mean value), spatial CVs were calculated for daily fields. Only days with a high mean precipitation were included, to avoid insignificant drizzle and events covering only a small fraction of the total area. A threshold of 15 mm day^{-1} turned out to generate large enough samples (for robust statistics) of days with significant precipitation events. For each selected day, CV was calculated from all gridcell values in the matrix after which monthly mean CVs were calculated. At a resolution of 50 km, PTHBV exhibits a very distinct annual cycle with a low CV in the winter, reflecting smooth, frontal-type precipitation fields, and a summer peak reflecting the presence of convective cells substantially increasing the variability (Fig. 2b). RCA3 reproduces this cycle well, except for an underestimated CV in April and in the autumn. At higher resolutions, the shape of the annual cycle is essentially retained, but it is shifted upward, reflecting an increased variability as the level of spatial detail increases. The difference between 12 and 25 km is rather small, and in some months the 25-km CV is similar to or even higher than (August) the 12-km CV (Fig. 2b). Also at these resolutions, RCA3 captures the properties of the PTHBV data well.

Overall, these analyses have demonstrated that RCA3 is capable of reproducing the spatial structure and variability of precipitation in the region at the daily scale. In light of this, it may be assumed that observed local, short-term precipitation statistics may also be approached as spatial resolution increases. This assumption is investigated in the following.

3. Methods

To assess the RCM-simulated precipitation, we use a range of statistical evaluation metrics, divided into three categories: conventional statistics, IDF curves, and event-based statistics.

a. Conventional statistics

These included the following metrics: total accumulated precipitation P^{tot} (mm); maximum precipitation intensity I^{max} [mm (30 min)$^{-1}$]; wet fraction WF, that is, the fraction of 30-min time steps with precipitation > 0.1 mm (%); precipitation intensity in the wet fraction I^{WF} [mm (30 min)$^{-1}$]; and standard deviation of precipitation intensity in the wet fraction [std dev(I^{WF}); mm (30 min)$^{-1}$].

It should be emphasized that the wet fraction, as well as the wet spell properties described below, are influenced

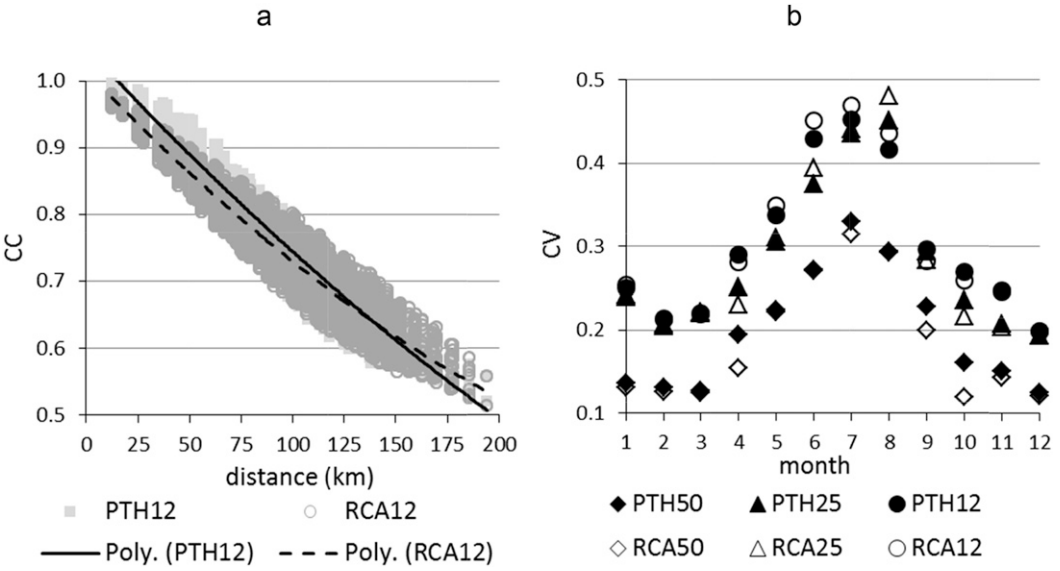

FIG. 2. For the Växjö box in PTHBV and RCA3 (a) CC as a function of separation distance at 12- km resolution where the lines represent polynomial regressions and (b) monthly averages of daily spatial CV at resolutions of 50, 25, and 12 km.

by the definitions of wet and dry time step. For example, using a cutoff threshold other than 0.1 mm for the RCA3 data will generate different wet fractions and different sets of wet spells, which will agree more or less with the observed values (e.g., Bärring et al. 2006). Further, it could be considered to express the cutoff threshold as a function of spatial resolution. Here, as mentioned above, in order to facilitate interpretation, we use the same lower limit for nonzero precipitation in all data (0.1 mm) and discuss the implications of this choice whenever relevant.

b. IDF curves

For each time series, annual maxima of durations d = 30 min, 1 h, 3 h, 6 h, 12 h, and 1 day were calculated by using a moving time window (note that in this case, "duration" does not imply from the beginning to the end of an event, but only the length of the time window). For all durations, the Gumbel distribution was fitted to these sets of 14 annual maxima. The Gumbel distribution belongs to the generalized extreme value (GEV) family of distributions, whose members are defined by the value of the shape parameter θ. The case $\theta = 0$ gives a Gumbel distribution, $\theta > 0$ gives a Fréchet distribution, and $\theta < 0$ gives a Weibull distribution (also called GEV types I, II, and III; WMO 1981). The Gumbel distribution has previously been found suitable for 30-min precipitation extremes from RCA3 (Olsson and Foster 2013), and for consistency, it is used here to model also the extremes in the observed time series. The goodness of fit was evaluated by visual inspection (Fig. 3) and was determined to be sufficient for using the Gumbel distribution also for the observations. From the fitted Gumbel distributions, 10-yr intensities corresponding to each duration $I10_d$ were estimated [mm (30 min)$^{-1}$].

c. Event-based statistics

In an event-based analysis of precipitation time series, a minimum dry period needs to be defined that determines if two adjacent wet periods are to be considered independent or part of the same wet spell. Although some theoretical methods have been developed for this purpose (e.g., Restrepo-Posada and Eagleson 1982), here we used a minimum dry period of 2 h, which is an established value in analyses of Swedish high-resolution precipitation data (e.g., Hernebring 2006). Thus, wet spells were allowed to contain dry periods of up to 1.5 h.

The identified wet spells were characterized in terms of three metrics:

number of wet spells WS^{nr};
wet spell length WS^{len}, that is, from the first time step preceded by at least 2 dry hours to the last time step succeeded by at least 2 dry hours (h); and
wet spell depth WS^{dep}, that is, accumulated precipitation depth from all time steps included in the wet spell (mm). Each wet spell was assigned to the month of its central time step.

d. Application to data

All the above calculations were performed for each observed time series. Conventional and event-based

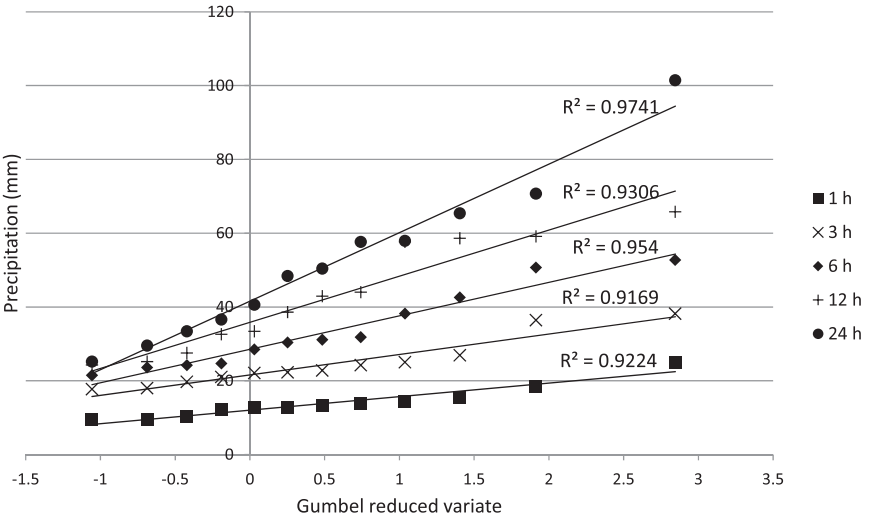

FIG. 3. Example of Gumbel fits (lines) to annual max of different durations (symbols) for the Växjö station.

statistics were calculated for each month in the period and then averaged over all 14 years, that is,

$$M_m^{\text{obs}} = \frac{\sum_{y=1995}^{2008} M_{y,m}^{\text{obs}}}{14}, \tag{1}$$

where $M_{y,m}^{\text{obs}}$ represents one of the conventional or event-based metrics M described above, calculated for observations in year y and month m.

Concerning the RCA3 data, for conventional and event-based statistics the calculations were performed in a similar way as for the observations [Eq. (1)] for each gridcell time series separately, after which the results were averaged over all grid cells of the same size in each location's matrix, that is,

$$\overline{M}_m^{\text{RCA}} = \frac{\sum_{c=1}^{N}\sum_{r=1}^{N} M_{m,c,r}^{\text{RCA}}}{N^2}, \tag{2}$$

where $\overline{M}_m^{\text{RCA}}$ denotes a metric M calculated using RCA3 data by spatially averaging over all columns c and rows r in the $N \times N$ matrix corresponding to a certain RCA3 resolution. Similarly, the 10-yr intensities $I10$ were averaged according to

$$\overline{I10}_d^{\text{RCA}} = \frac{\sum_{c=1}^{N}\sum_{r=1}^{N} I10_{d,c,r}^{\text{RCA}}}{N^2}, \tag{3}$$

where $\overline{I10}_d^{\text{RCA}}$ denotes the average intensity for duration d.

The comparison between observations and RCA3 data is made mainly in terms of relative bias B of the different statistics. For conventional and event-based statistics, bias is calculated as

$$B_m = 100\left[\frac{(\overline{M}_m^{\text{RCA}} - M_m^{\text{OBS}})}{M_m^{\text{OBS}}}\right], \tag{4}$$

and for $I10$ bias is calculated as

$$B_d = 100\left[\frac{(\overline{I10}_d^{\text{RCA}} - I10_d^{\text{OBS}})}{I10_d^{\text{OBS}}}\right], \tag{5}$$

where B_m and B_d represent month- and duration-specific bias (%), respectively.

Besides this main approach, two sensitivity tests were performed in order to evaluate different aspects of the chosen methodology. One issue concerns the different RCM grid sizes used. As mentioned in section 2, all RCM data are treated as point-scale data despite representing different areas and, in turn, different precipitation characteristics. To assess any statistical effect related only to the grid size and to understand the impact on, for example, wet spell characteristics, the data at resolutions 25, 12, and 6 km were mapped (averaged) to the 3×3 matrix at 50-km resolution and evaluated in terms of the above statistics. This way, the influence of spatial resolution on the results is eliminated and differences between the RCM runs may be assessed on equal terms.

Another issue concerns the different number of grid cells at the different resolutions, at each location ranging from 9 at 50 km to 576 at 6 km, and any related impact on the results. In a second sensitivity test, this was investigated

by using a 3 × 3 matrix at all RCM resolutions. Thus, at each gauge, a variable surrounding area ranging from 22 500 km^2 at 50 km down to 324 km^2 at 6 km was used. In terms of a neighborhood approach, this amounts to using a 1.5 RCM gridcell radius in the evaluation, as a complement to the fixed 75-km radius (i.e., 1.5 50-km cells) used in the main approach.

4. Results

The total result of the study is summarized in Table 1. Here, the relative bias of all statistics considered is given, averaged over the whole 14-yr period and all seven locations. The dependency on location is rather weak, but in relative terms the bias appears overall consistent within the area studied. Exceptions from this general tendency are noted below. However, there is in general a pronounced seasonal dependency of the bias. In sections 4a and 4c below, the results in Table 1 are complemented with graphical evaluations of the statistics' annual cycle, both in the reference observations and in the RCA3 bias. Concerning the latter, the results for each month have been averaged over all 14 years of data and all seven locations. As the IDF curves are based on annual maxima, seasonal dependency is not relevant. There is, however, a clear dependency on duration (Table 1) and this is thus illustrated in the graphical evaluation (section 4b).

TABLE 1. Values of B (%) in all statistics considered, averaged over the whole 14-yr period and all seven locations.

		50 km	25 km	12 km	6 km
Conventional statistics	P^{tot}	+5	+4	+10	+22
	I^{max}	−55	−45	−35	−2
	WF	+61	+55	+59	+64
	Avg (I^{WF})	−34	−31	−29	−22
	Std dev (I^{WF})	−62	−53	−46	−15
IDF curves (10 yr)	30-min intensity	−86	−75	−50	−13
	1-h intensity	−84	−68	−41	−11
	2-h intensity	−76	−53	−20	0
	3-h intensity	−68	−40	−9	+7
	6-h intensity	−53	−25	−6	+6
	12-h intensity	−50	−27	−16	+1
	24-h intensity	−54	−35	−25	−6
Event-based measures	WS^{nr}	+12	+13	+16	+23
	WS^{dep}	−1	−8	−12	−7
	WS^{len}	+64	+30	+24	+41

a. Conventional statistics

In southern Sweden, the largest amounts of precipitation generally fall during summer (e.g., Kjellström et al. 2011), and this is overall reflected in the observations used here (Fig. 4a). The station Göteborg, however, differs from the other stations in that monthly totals during autumn and early winter equal to or even exceeded the summer totals in the 14-yr period considered. This feature was verified in the long-term climatology for Göteborg (1961–90), which also exhibits higher precipitation totals in autumn than in summer.

At 50-km resolution, the RCA3 bias is generally positive with a value up to +20%, but there are also months with a similar negative bias (Fig. 4b) and where no seasonal pattern is apparent. Averaged over all months, a slight positive bias of +5% is found (Table 1). The results may be compared with Kjellström et al. (2011), who evaluated seasonal totals from the same model run (period 1961–90) with gridded observations (E-OBS; Haylock et al. 2008). In southern Sweden they found a slight positive bias in winter, in agreement with our results, but a more pronounced overestimation in summer. This is likely due to an underestimation of extreme precipitation in E-OBS (Hofstra et al. 2009), which has a larger influence on the summertime precipitation in this part of Europe. A comparison between the station measurements and E-OBS confirmed this underestimation also in the monthly totals.

The results are overall similar at 25 km, but at the highest resolutions the bias becomes more positive, reaching +25% at 6 km. At this resolution there are no months with a negative bias, but high values between +30% and +50% are found for August, October, January, and February (Fig. 4b). This pattern is overall consistent in all locations, except that Stockholm has a smaller positive bias in January and February. Averaged over all months and resolutions, the bias is largest in Lidköping (+21%) and smallest in Göteborg (−4%); the latter is likely related to the high precipitation amounts in the observations (Fig. 4a). The inconsistent bias between the stations, especially for coastal and inland stations, could point to a model deficiency. It could also be an effect of ocean grid cells being included in the investigated area, as these can have rather different climate due to, for example, orographic precipitation. Inspection of time series from single inland grid cells close to the stations, however, indicates an overall similar bias as for the total gridcell matrices.

The region's climatology described in section 2 implies a prevalence of frontal, long-lasting, widespread precipitation of low-to-moderate intensity in winter and convective, short-lived, localized, high-intensity storms in summer. Thus the highest intensities are expected in summer, which is reflected in the observations of maximum 30-min precipitation, exhibiting a distinct annual cycle with a peak in July–August (Fig. 5a). There is a limited variation between the locations, but Göteborg stands out with the highest annual maximum (in August) as well as the highest value in most other months.

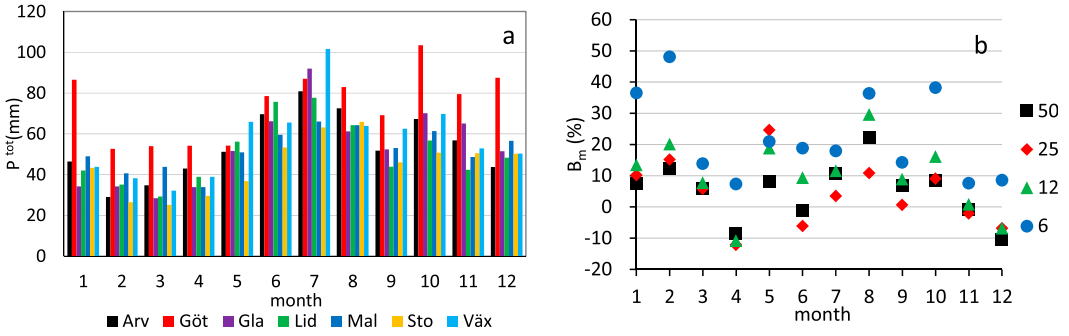

FIG. 4. (a) Observed annual cycle of P^{tot} at each location averaged over 1995–2008. (b) Average annual cycle B_m in the RCA3 simulations with resolutions of 50, 25, 12, and 6 km, averaged over the seven locations.

In the 50-km RCA3 simulation, the bias has a distinct annual cycle (Fig. 5b), being smallest in winter (~−40%) and largest in summer (~−70%), with an average value of −53% (Table 1). Generally, a pronounced negative bias is expected in light of the large difference in scale between the point observations and the RCA3 grid. The inherent spatial averaging in the latter will by construction lead to lower maxima. The annual cycle of the bias reflects the expected annual cycle of areal reduction factors (ARFs), with higher ARFs (i.e., lower reduction) in winter when the maxima are related to large-scale fields and vice versa in summer when the maxima are localized (e.g., Allen and DeGaetano 2005). A further source of the higher summer bias is likely limitations in the parameterization of convective precipitation in RCA3.

As the RCA3 resolution increases to 25 and 12 km, the annual cycle gradually improves, mainly because of a decreased bias in summer (Fig. 5b). This implies that, in terms of the highest intensities, the increased resolution is mainly beneficial for improving the reproduction of localized summer maxima, although a substantial negative bias still exists at 12 km. At 6 km the total bias is only −2% (Table 1), but Fig. 5b reveals that this is a clear case of compensating errors. As compared with the 12-km run, there is in the 6-km run a general bias reduction in spring and summer, although it is similar to the 12-km run in July and August. In late autumn (October–November), the 6-km run is essentially unbiased, but in winter there is a pronounced positive bias in the monthly maximum intensity, especially in January–February (Fig. 4b). This implies that the simulated monthly maximum intensities in the 6-km run are of a similar magnitude [3–4 mm $(30\,\text{min})^{-1}$] throughout the year. As was the case for total precipitation, the pattern is similar in all stations but less pronounced in Stockholm.

At a 30-min resolution, the wet fraction in the observations range from 10%–12% of the time during late autumn and winter to 5%–6% in summer, with limited variation between the locations (Fig. 6a). This reflects the dominant mechanisms and their associated durations: long, frontal-type events in autumn and winter and short, convective-type events in summer. As a spatial average by construction has a larger probability of precipitation than a point, the RCA3 data are expected to have a positive bias, which is also the case (Fig. 6b). Between November and April, the bias is ~+30% and almost independent of the RCA3 resolution. In summer, the bias reaches from +100% to +150% and generally increases with increasing resolution. This might be related to drizzle and the dependency on the definition of

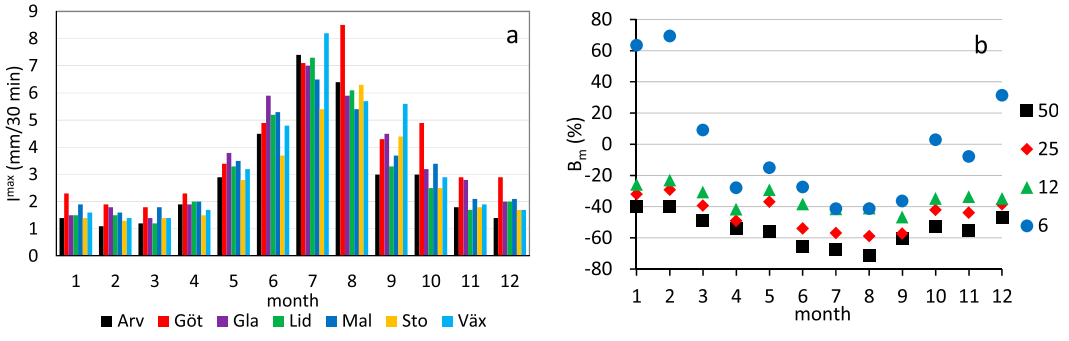

FIG. 5. As in Fig. 4, but for I^{max}.

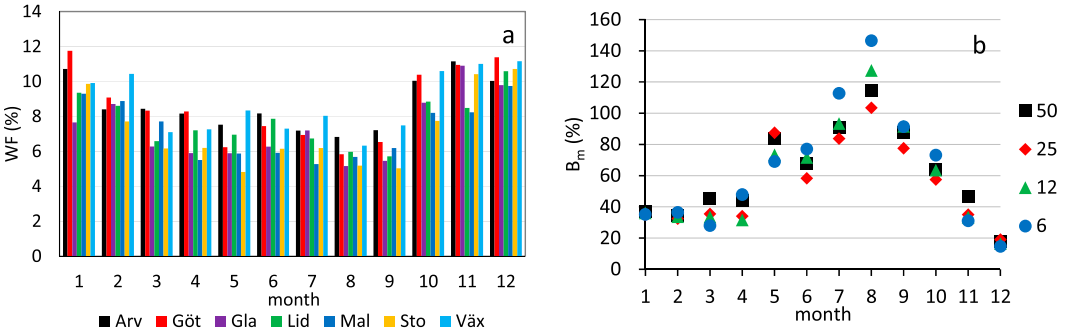

FIG. 6. As in Fig. 4, but for WF.

a wet time step. For example, when increasing the limit of what is considered wet from 0.1 to 0.5 mm, the bias turns negative in winter but remains positive in summer. This is partly an effect of the inherent spatial averaging in the models. This averaging shifts the intensity distribution toward lower intensities, increasing the probability of occurrence of lower intensities and decreasing the probability of higher intensities. The point of transition determines the intensity for which the wet fraction changes sign when comparing point data to spatial averages. This point is not straightforward to calculate as it depends on the spatial structure of the precipitating system. Besides this statistical effect, there is a tendency for RCA3 to produce excessive drizzle, which further increases the probability of low-intensity rainfall. This too can have large consequences for the wet fraction bias and might be a larger problem for summertime precipitation if produced by the convective parameterization.

As the monthly total generally peaks in summer (Fig. 4a), when the wet fraction is at its minimum (Fig. 6a), the mean precipitation intensity during wet periods has an even more distinct summer peak than the monthly totals (Fig. 7a). As for the monthly totals, the highest values are generally found in the Göteborg station.

Concerning RCA3, as the bias in monthly totals is relatively limited (Fig. 4b) but the wet fraction is clearly overestimated (Fig. 6b), the intensity during wet periods is underestimated (Fig. 7b). In summer, the underestimation approaches −50% and is independent of the RCA3 resolution. Also during the rest of the year, the result is similar for resolutions of 50, 25, and 12 km, but for 6 km the underestimation is less pronounced. In February the intensity is even overestimated in the 6-km run; the strongly overestimated February total in the 6-km run (Fig. 4b) is thus a combined effect of overestimations of both wet fraction and wet intensity. There is some variability between the stations. Averaged over all months and resolutions, the bias is smallest in Arvika (−19%) and largest in Göteborg (−38%).

The standard deviation of the wet fraction intensity is very similar to the maximum 30-min intensity (Fig. 5), both in terms of the annual cycle in the observations (Fig. 8a) and the character of the RCA3 bias (Fig. 8b). Thus, the standard deviation is clearly underestimated in RCA3, with a magnitude that decreases with increasing resolution (Table 1). A notable feature is the change to a strong overestimation in the 6-km RCA3 run during January–February.

b. *IDF curves*

In the observations, the 10-yr intensity associated with 1-day duration ranges between 1.94 (Lidköping) and 3.45 mm h^{-1} (Göteborg) (Fig. 9a). These values correspond to daily totals of 46.5 and 82.9 mm, respectively. Averaged over all stations, the 10-yr 1-day duration total is 59.0 mm. This can be compared with the study by Wern and German (2009), who found an average value for Sweden of 53.4 mm by analyzing precipitation data from 114 stations during the same period as in this study (1995–2008). Also, for shorter durations, the 10-yr intensities in this study are higher than in Wern and German (2009), by ~20% on average. This partly reflects a tendency to higher values in southern than in northern Sweden (Wern and German 2009). The difference may also be a result of the fact that Wern and German (2009) used a nonzero value of the θ parameter (section 3), calculated as an average value from individual fitting to all stations.

Concerning the RCA3 simulation at 50-km resolution, there is a strong negative bias (Fig. 9b) that, as discussed in connection with Fig. 5, is a natural consequence of spatial averaging. The underestimation at duration 30 min, −86% (Table 1), can be compared with the value −72% for the maximum 30-min intensity in summer (August; Fig. 5b). The more unusual 10-yr intensity is thus underestimated to a larger degree than the

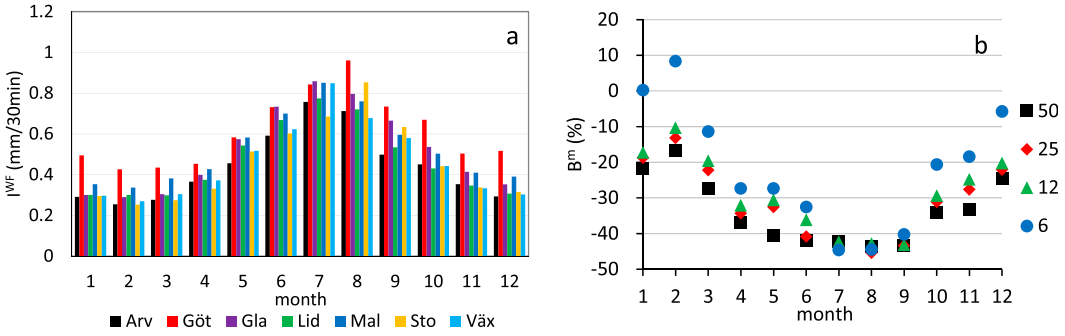

FIG. 7. As in Fig. 4, but for I^{WF}.

annual average maximum intensity. There is a clear trend of decreasing bias with increasing duration (Table 1). This is a likely reflection of the fact that while the shortest-duration extremes are often related to very localized precipitation fields, longer-duration extremes are gradually more likely to be associated with larger-scale fields (e.g., Olsson et al. 2014). As RCA3 is able to better represent the latter, the pattern in Fig. 9b may be expected.

Increasing the resolution gradually reduces the bias. The increase from 50 to 25 km mainly reduces the bias for the longer durations considered. This might be due to more realistic large-scale circulation at the higher resolution that affects the paths of large-scale fronts. The increase from 25 to 12 km mainly reduces the bias for the shorter durations, which might be due to better-resolved small-scale processes related to orography and convective processes. At 6 km, the 10-yr intensities are almost unbiased for durations between 2 h and 1 day (Fig. 9b, Table 1). For the shortest durations, a bias from −10% to +15% still remains.

The variations between different locations are illustrated in Figs. 9c and 9d, representing the two extreme cases with respect to how the 6-km RCA3 IDF curve matches the observations at short durations. In Stockholm, the 6-km IDF curve strongly underestimates the shortest-duration extremes, by ~50% (Fig. 9c). In Malmö, however, they are overestimated by ~30% (Fig. 9d). Also, for the longer durations, the bias ranges approximately ±40% for the different stations. It should be remarked that a pronounced statistical scatter is expected in the procedure of fitting the Gumbel distribution to (a rather limited set of) annual maxima.

c. *Event-based statistics*

In the observations, the number of wet spells per month is smallest in spring (~5) and largest in summer (~8; Fig. 10a). Generally, the Göteborg station registers the largest number of wet spells; in late autumn and early winter there are 2–3 more wet spells per month than in the other stations.

RCA3 generally overestimates the number of wet spells (Fig. 10b). Overall, the overestimation is of similar magnitude throughout the year, although there are substantial month-to-month variations. In actual numbers, the overestimation is limited. The average bias at 50-km resolution (+12%; Table 1) corresponds to 0.67 excessive wet spells per month and year, that is, for each month, two excessive wet spells are generated over a 3-yr period. The bias increases with increasing resolution, up to +23% at 6 km (Table 1), that is, the higher the resolution, the more wet spells are generated. As noted above (section 3), the definition of the wet spells is dependent on the gauge precision (in the observations)

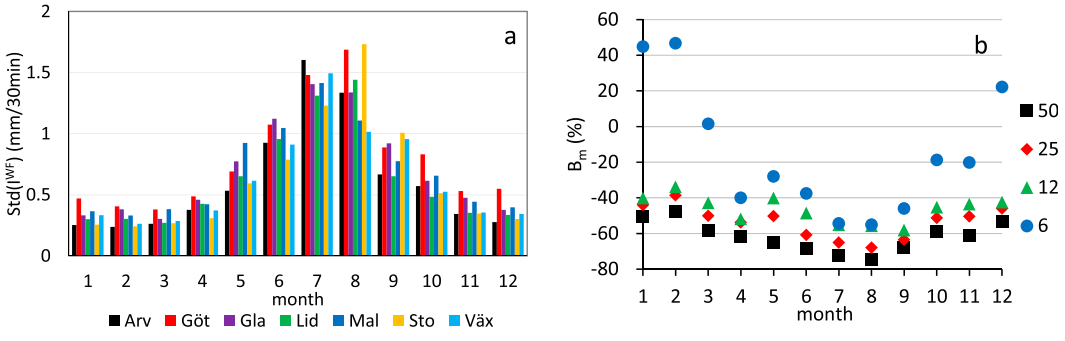

FIG. 8. As in Fig. 4, but for std dev (I^{WF}).

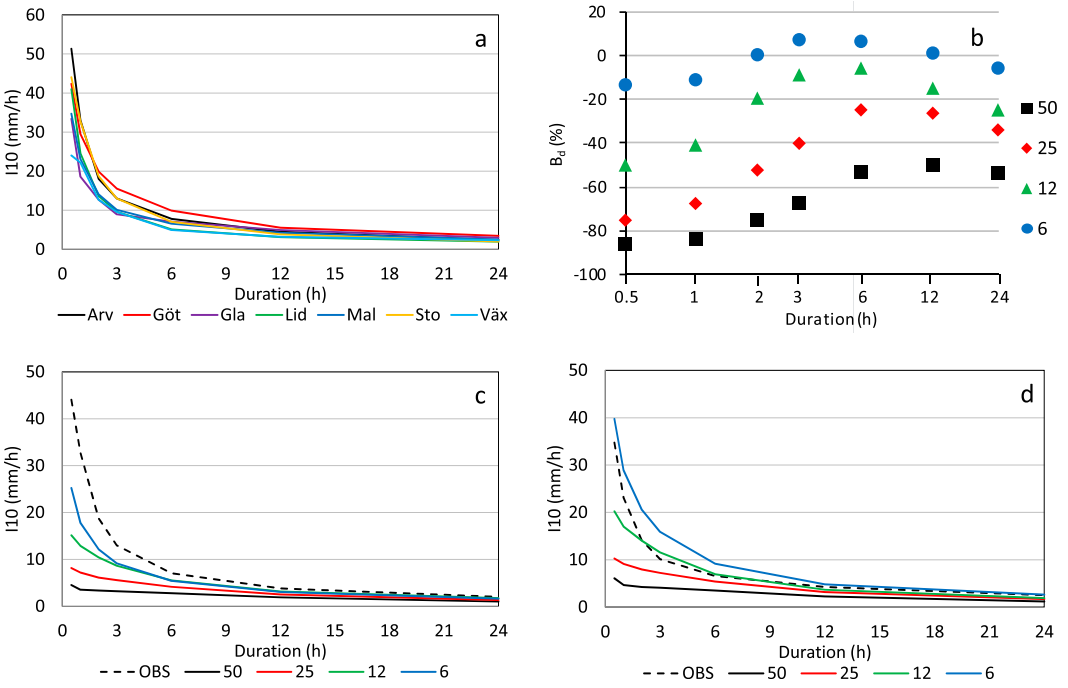

FIG. 9. (a) The 10-yr IDF curves calculated from observations at each location and (b) B_d in the RCA3 simulations averaged over the seven locations. Observed and simulated IDF curves for (c) Stockholm and (d) Malmö.

and the cutoff limit separating between wet and dry time steps (in the RCM data). Thus, for this statistic there also is a sensitivity issue with the results that is difficult to account for. For example, a weak convective event might be counted in one grid cell at a high resolution, but when averaged on a coarser grid, it might be below the wet limit and thus not counted. There is also the influence of excessive drizzle that might be affecting results.

In the observations, the average depth of wet spells is generally 5–6 mm in winter and 8–9 mm in summer (Fig. 11a). At 50-km resolution, the RCA3 bias is generally within ±10% (Fig. 11b) with an average of −1% (Table 1). There is a weak tendency of overestimated depths in winter and underestimated depths in spring and summer. Increasing the resolution leads to a slight negative bias with a principally similar annual pattern. At 6 km there is larger spread in the bias across different months (~±25%; Fig. 11b).

The observed average length of wet spells is ~8 h in the winter half-year but drops to 4–5 h in summer, reflecting the occurrence of short, convective-type rainfall events (Fig. 12a). In this case, the Arvika station stands out with the longest average wet spell length during most of the year.

At 50-km resolution, there is a strong positive bias in the RCA3 simulation, ranging from +35% in winter to more than +100% in summer. This is at least partly an effect of spatial averaging; a precipitation field will remain longer within a certain area than over a certain

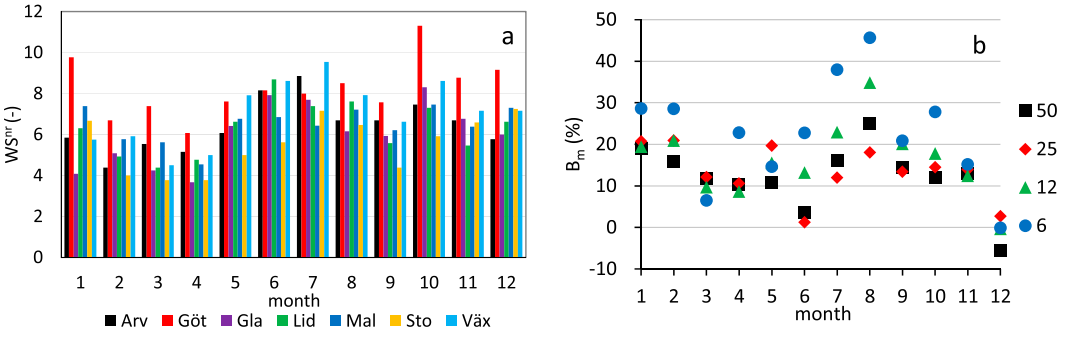

FIG. 10. As in Fig. 4, but for WS^{nr}.

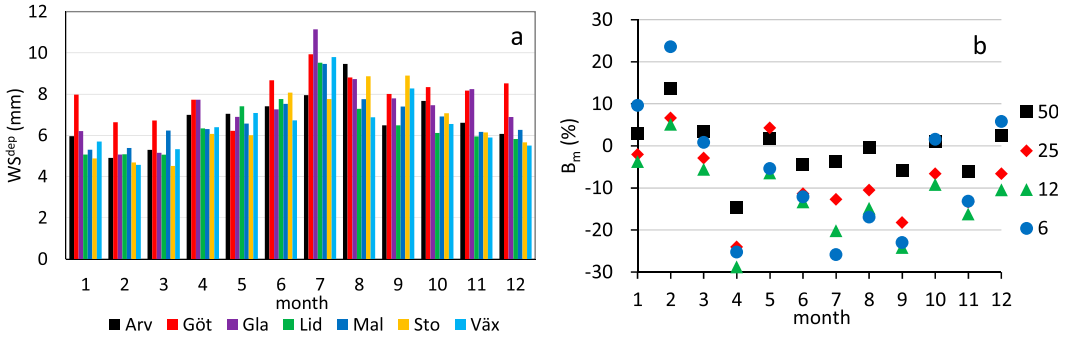

FIG. 11. As in Fig. 4, but for WS^{dep}.

point. In relative terms, this effect will increase with decreasing wet spell length, in line with the results in Fig. 12b. Another effect is possible prolongation of the wet spells due to drizzle before or after the actual event. The essentially unbiased reproduction of the observed wet spell depths in the 50-km RCA3 resolution (Table 1) is thus actually generated by longer wet spells (Fig. 12b) with a lower average intensity (Fig. 7b).

As the RCA3 resolution increases to 25 and 12 km, the wet spell length bias is substantially reduced. At 12 km, the bias is ~+15% in winter and ~+35% in summer (Fig. 12b). Even if this is accompanied by a slight increase in the wet spell depth bias (Table 1), it indicates that the representation of wet spells at 12-km resolution is much closer to the point observations than in the lower-resolution runs. At 6 km, however, the RCA3 bias again increases, most notably in summer, possibly because of an increased drizzle effect.

d. Sensitivity tests

In the first sensitivity test described above, the 25-, 12-, and 6-km data were mapped to 50-km resolution in order to verify the expected effects of spatial coarse graining on the precipitation statistics and to assess the impact of using a fixed cutoff (threshold = 0.1 mm) to separate between wet and dry time steps. Generally, the descriptive statistics and IDF curves change as expected with coarse graining. Monthly totals do not change, except for negligible numerical effects related to the regridding. Maximum intensity, standard deviation, and IDF values are all reduced, to an increasing degree with increasing original resolution. The reduction is most pronounced in summer, reflecting the small-scale nature of convective precipitation.

The wet fraction increases with coarse graining, to an increasing degree with increasing original resolution, and most notably in summer. Thus, the wet fraction bias increased substantially during summer compared with the resolution-specific results (Fig. 6b), reaching from +200% to 250% for the 6-km data mapped to 50 km. This suggests a situation where high intensities are generated at the higher resolutions, and when averaged to 50 km, they produce averages above the wet threshold. Concerning summer wet spells, their number in the sensitivity test gives a result overall similar to the resolution-specific bias (Fig. 10b). Instead, the increased wet fraction bias is accompanied by a similar increase of the wet spell length bias for the higher-resolution runs in the sensitivity test. Thus, the high intensities at the higher resolutions are clustered into wet spells that correspond to the lower-resolution ones.

In the second sensitivity test, precipitation statistics were calculated using a 3 × 3 matrix at all RCM resolutions instead of the fixed 150 × 150 km^2 area used in the main approach. The results from the 3 × 3 matrix calculations were virtually identical to the results shown in sections 4a–4c above. The very small differences found had no apparent systematic features and are most likely statistical scatter. Thus, the choice of area surrounding each gauge and the resulting different number of grid cells at the different RCM resolutions do not appear to have influenced the results.

5. Summary and conclusions

The correspondence between observed high-resolution (30 min) precipitation statistics at point scale in southern Sweden and analysis-driven RCA3 simulations with spatial resolutions between 50 and 6 km was investigated. The main findings include the following.

- For conventional statistics, no positive impact of a higher RCA3 resolution on monthly totals and wet fraction could be seen, but for short-term variability and maxima, the agreement with observations increased overall with increasing RCA3 resolution.
- For the 10-yr IDF curves, increasing the RCA3 resolution substantially improved the correspondence with observations, and at 6 km the absolute bias is <15% for all durations considered (30 min to 24 h).

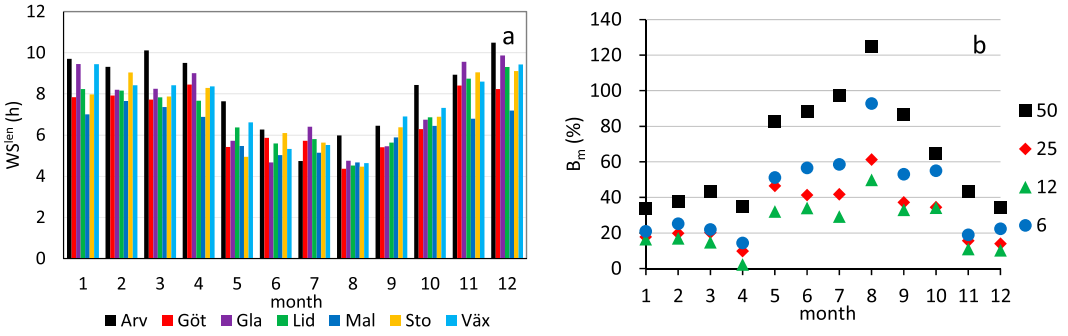

FIG. 12. As in Fig. 4, but for WS^{len}.

- For event-based statistics, a higher RCA3 resolution did not improve agreement with observation-based estimates.

In total, the main added value of a higher resolution is better reproduction of summer maxima (which are reflected in the IDF curves) and summer wet spell durations, which is in agreement with previous studies (e.g., Kendon et al. 2012; Prein et al. 2013). A general tendency found here is that the bias is steadily reduced, or remains essentially unchanged, when going from 50 to 25 and 12 km. The further increase to 6 km, however, in some respects increases the bias in certain seasons. One clear example is winter maxima, which change from being substantially underestimated at 12 km to being overestimated (to an even higher degree) at 6 km. A possible explanation for this can be generation of too deep lows in the model at 6 km, causing more extreme winter storms. An in-depth analysis of such phenomena was out of scope for the current paper but should be undertaken in follow-up studies. Another example is wet spell length in summer, which is clearly more overestimated at 6 than at 12 km. The wet spell length might be strongly affected by excessive drizzle, possibly to an increasing degree with increasing resolution in combination with a resolution effect on the definition of a wet time step.

The close reproduction of the observed IDF curves in the 6-km RCA3 run indicates an ability of the model to generate low-frequency subdaily extremes of the same order of magnitude as in point observations. As such extremes have a strong societal impact, for example, by causing urban flooding and triggering landslides and debris flow, accurate estimation by climate modeling would be a significant advancement. An obvious application is assessment of future changes, but historical simulations can also be valuable in light of the limited availability of short-term precipitation data in many parts of the world. Our results indicate that this prospect is attainable at resolutions of ~5 km, although much further validation remains.

It should be emphasized that point-scale (i.e., station) time series have been used in this evaluation and that deviations between observed and simulated data for many of the metrics used reflect both RCM bias and scale effects between areal and point precipitation. Although climate model output is sometimes directly compared with single-station data (e.g., Willems and Vrac 2011; Mishra et al. 2012; Tripathi and Dominguez 2013), it is more common to use observation-based areal estimates. Although in principle allowing for evaluation of RCM bias without having to consider scale effects, areal precipitation estimates are substantially more uncertain than point observations, regardless of, for example, measurement device and interpolation method. We believe complementary assessment of RCM performance against both point and areal data is needed. A difficulty when comparing point and areal precipitation concerns the cutoff threshold used to separate between wet and dry time steps, which is an important variable for the assessment of model performance in terms of wet fraction and event-based characteristics. Our practical approach of using the gauge sensitivity as RCM cutoff at all spatial resolutions is an ad hoc solution, and a more systematic treatment of this issue is desirable in future research.

Acknowledgments. The study was mainly funded by the Swedish Research Council Formas, through the HYDROIMPACTS2.0 project, and the Foundation for Strategic Environmental Research (MISTRA), through the Mistra-SWECIA project. Additional funding from Tokyo Metropolitan University (TMU), Japan Society for the Promotion of Science (JSPS), and the Scandinavia–Japan Sasakawa Foundation allowed Jonas Olsson to perform complementary work during visits at TMU. Warm thanks are extended to Grigory Nikulin, Kean Foster, and Lennart Simonsson for help with data extraction and processing. Comments from three anonymous reviewers helped improve the original manuscript.

REFERENCES

Allen, R. J., and A. T. DeGaetano, 2005: Areal reduction factors for two eastern United States regions with high

rain-gauge density. *J. Hydrol. Eng.,* **10,** 327–335, doi:10.1061/(ASCE)1084-0699(2005)10:4(327).

Bärring, L., T. Holt, M.-L. Linderson, M. Radziejewski, M. Moriondo, and J. P. Palutikof, 2006: Defining dry/wet spells for point observations, observed area averages, and regional climate model gridboxes in Europe. *Climate Res.,* **31,** 35–49, doi:10.3354/cr031035.

Berg, P., Ch. Moseley, and J. O. Haerter, 2013a: Strong increase in convective precipitation in response to higher temperatures. *Nat. Geosci.,* **6,** 181–185, doi:10.1038/ngeo1731.

——, S. Wagner, H. Kunstmann, and G. Schädler, 2013b: High resolution regional climate model simulations for Germany: Part I—Validation. *Climate Dyn.,* **40,** 401–414, doi:10.1007/s00382-012-1508-8.

Chan, S. C., E. J. Kendon, H. J. Fowler, S. Blenkinsop, C. A. T. Ferro, and D. B. Stephenson, 2013: Does increasing the spatial resolution of a regional climate model improve the simulated daily precipitation? *Climate Dyn.,* **41,** 1475–1495, doi:10.1007/s00382-012-1568-9.

Dai, A., 2001: Global precipitation and thunderstorm frequencies. Part I: Seasonal and interannual variations. *J. Climate,* **14,** 1092–1111, doi:10.1175/1520-0442(2001)014<1092:GPATFP>2.0.CO;2.

Haerter, J. O., P. Berg, and S. Hagemann, 2010: Heavy rain intensity distributions on varying time scales and at different temperatures. *J. Geophys. Res.,* **115,** D17102, doi:10.1029/2009JD013384.

Haylock, M. R., N. Hofstra, A. M. G. Klein Tank, E. J. Klok, P. D. Jones, and M. New, 2008: A European daily high-resolution gridded data set of surface temperature and precipitation for 1950–2006. *J. Geophys. Res.,* **113,** D20119, doi:10.1029/2008JD010201.

Heinrich, G., and A. Gobiet, 2012: The future of dry and wet spells in Europe: A comprehensive study based on the ENSEMBLES regional climate models. *Int. J. Climatol.,* **32,** 1951–1970, doi:10.1002/joc.2421.

Hernebring, C., 2006: Design storms in Sweden then and now (in Swedish). VA-forsk Publ. 2006–04, Svenskt Vatten, Stockholm, Sweden, 85 pp.

Hofstra, N., M. Haylock, M. New, and P. D. Jones, 2009: Testing E-OBS European high-resolution gridded data set of daily precipitation and surface temperature. *J. Geophys. Res.,* **114,** D21101, doi:10.1029/2009JD011799.

Johannessen, T. W., 1970: The climate of Scandinavia. *Climates of Northern and Western Europe,* C. C. Wallén, Ed., World Survey of Climatology, Vol. 5, Elsevier, 23–80.

Johansson, B., 2000: Areal precipitation and temperature in the Swedish mountains: An evaluation from a hydrological perspective. *Nord. Hydrol.,* **31,** 207–228.

——, and D. Chen, 2003: The influence of wind and topography on precipitation distribution in Sweden: Statistical analysis and modeling. *Int. J. Climatol.,* **23,** 1523–1535, doi:10.1002/joc.951.

Jones, C., U. Willén, A. Ullerstig, and U. Hansson, 2004: The Rossby Centre regional atmospheric climate model part I: Model climatology and performance for the present climate over Europe. *Ambio,* **33,** 199–210.

Kain, J. S., and J. M. Fritsch, 1993: Convective parameterizations for mesoscale models: The Kain–Fritsch scheme. *The Representation of Cumulus Convection in Numerical Models, Meteor. Monogr.,* No. 46, Amer. Meteor. Soc., 165–170.

Kendon, E. J., N. M. Roberts, C. A. Senior, and M. J. Roberts, 2012: Realism of rainfall in a very high-resolution regional climate model. *J. Climate,* **25,** 5791–5806, doi:10.1175/JCLI-D-11-00562.1.

Kjellström, E., and Coauthors, 2005: A 140-year simulation of the European climate with the new version of the Rossby Centre regional atmospheric climate model (RCA3). SMHI Rep. 108, Swedish Meteorological and Hydrological Institute, Norrköping, Sweden, 54 pp.

——, G. Nikulin, U. Hansson, G. Strandberg, and A. Ullerstig, 2011: 21st century changes in the European climate: Uncertainties derived from an ensemble of regional climate model simulations. *Tellus,* **63A,** 24–40, doi:10.1111/j.1600-0870.2010.00475.x.

Maidment, D. R., Ed., 1993: *Handbook of Hydrology*. McGraw-Hill, 1424 pp.

Mishra, V., F. Dominguez, and D. P. Lettenmaier, 2012: Urban precipitation extremes: How reliable are regional climate models? *Geophys. Res. Lett.,* **39,** L03407, doi:10.1029/2011GL050658.

Olsson, J., and K. Foster, 2013: Extreme short-term precipitation in climate projections for Sweden (in Swedish). SMHI Climatology Rep. 6, SMHI, Norrköping, Sweden, 21 pp.

——, K. Berggren, M. Olofsson, and M. Viklander, 2009: Applying climate model precipitation scenarios for urban hydrological assessment: A case study in Kalmar City, Sweden. *Atmos. Res.,* **92,** 364–375, doi:10.1016/j.atmosres.2009.01.015.

——, L. Simonsson, and M. Ridal, 2014: Rainfall nowcasting: Predictability of short-term extremes in Sweden. *Urban Water J.,* **11,** 605–615, doi:10.1080/1573062X.2013.847465.

Prein, A. F., A. Gobiet, M. Suklitsch, H. Truhetz, N. K. Awan, K. Keuler, and G. Georgievski, 2013: Added value of convection permitting seasonal simulations. *Climate Dyn.,* **41,** 2655–2677, doi:10.1007/s00382-013-1744-6.

Restrepo-Posada, P. J., and P. S. Eagleson, 1982: Identification of independent rainstorms. *J. Hydrol.,* **55,** 303–319, doi:10.1016/0022-1694(82)90136-6.

Samuelsson, P., and Coauthors, 2011: The Rossby Centre Regional Climate Model RCA3: Model description and performance. *Tellus,* **63A,** 4–23, doi:10.1111/j.1600-0870.2010.00478.x.

Trenberth, K. E., and Coauthors, 2007: Observations: Surface and atmospheric climate change. *Climate Change 2007: The Physical Science Basis,* S. Solomon et al., Eds., Cambridge University Press, 235–336.

Tripathi, O. P., and F. Dominguez, 2013: Effects of spatial resolution in the simulation of daily and subdaily precipitation in the southwestern US. *J. Geophys. Res. Atmos.,* **118,** 7591–7605, doi:10.1002/jgrd.50590.

van Roosmalen, L., J. H. Christensen, M. B. Butts, K. H. Jensen, and J. C. Refsgaard, 2010: An intercomparison of regional climate model data for hydrological impact studies in Denmark. *J. Hydrol.,* **380,** 406–419, doi:10.1016/j.jhydrol.2009.11.014.

Walther, A., J.-H. Jeong, G. Nikulin, C. Jones, and D. Chen, 2013: Evaluation of the warm season diurnal cycle of precipitation over Sweden simulated by the Rossby Centre regional climate model RCA3. *Atmos. Res.,* **119,** 131–139, doi:10.1016/j.atmosres.2011.10.012.

Wern, L., and J. German, 2009: Short-term precipitation in Sweden 1995–2008 (in Swedish). Meteorology Rep. 139/2009, SMHI, Norrköping, Sweden, 35 pp.

Willems, P., and M. Vrac, 2011: Statistical precipitation downscaling for small-scale hydrological impact investigations of climate change. *J. Hydrol.,* **402,** 193–205, doi:10.1016/j.jhydrol.2011.02.030.

——, J. Olsson, K. Arnbjerg-Nielsen, S. Beecham, A. Pathirana, I. Bülow Gregersen, H. Madsen, and V.-T.-V. Nguyen, Eds., 2012: *Impacts of Climate Change on Rainfall Extremes and Urban Drainage Systems*. IWA Publishing, 238 pp.

WMO, 1981: Selection of distribution types for extremes of precipitation. Operational Hydrology Rep. 15/WMO Publ. 560, World Meteorological Organization, Geneva, Switzerland, 64 pp.